J. Fluid Mech. (2003), *vol.* 489, *pp.* 239–267.
DOI: 10.1017/S002211200300510X Printed in the United Kingdom

Horizontal dispersion of a near-bed coastal plume

By DEREK A. FONG[1] AND MARK T. STACEY[2]

[1]Environmental Fluid Mechanics Laboratory, Department of Civil and Environmental Engineering, Stanford University, Stanford, CA 94305-4020, USA

[2]Department of Civil and Environmental Engineering, University of California-Berkeley, 509 Davis Hall, Berkeley, CA 94720-1710, USA

(Received 30 July 2002 and in revised form 28 February 2003)

The transport of scalars in the coastal ocean is considered through the analysis of a vertically constrained plume which disperses laterally. Observations of the plume are made using an autonomous underwater vehicle (AUV) operating in two modes: (i) repeated transects of the plume at a fixed distance from the source; and (ii) a large-scale mapping of the plume development. Together, these measurements define both the variability in the plume centreline (i.e. the meandering) and the growth of the plume around the centreline (i.e. the relative dispersion). The analysis of the measurements suggests that the meandering is well-described by a spatially uniform but temporally variable velocity field, indicating that large-scale flow structures dominate the centreline variability. The growth of the plume downstream is seen to follow a scale-dependent dispersion law, most likely of a compound structure: a 4/3-law in the near field, and a scale-squared law in the far field. This transition between dispersion laws is consistent with the transition from three-dimensional turbulence structures to two-dimensional eddies, which is due to the constraints imposed on the vertical dimension at the site. Comparing the two dispersion processes, the effective dispersion created by meandering is found to be comparable with or larger than the relative dispersion in the near field; but in the far field, the relative dispersion is found to dominate considerations of overall dispersion.

1. Introduction

The dispersion of scalars in the environment determines the distribution and concentration of contaminants, nutrients and other flow constituents, such as larvae. Determining the scalar distribution downstream from a point source is an important step in establishing the environmental implications of scalar releases, whether the releases are natural or accidental (see e.g. Hill 1991 or Roberts 1999).

Dynamically, advection is likely to dominate the transport in the primary flow direction, while the lateral and vertical structure and the temporal variability of the plume are determined by environmental dispersion. Frequently, the vertical dimension is constrained, either by the presence of boundaries, as in the case of the coastal ocean, or by a boundary and a stratified layer, as would occur in the lower atmosphere or the surface layer of the ocean. Frequently, well-mixed conditions can be reached quickly in the vertical direction and the dispersion of scalars will occur primarily in the lateral horizontal direction, orthogonal to the dominant advective direction.

Under the action of random perturbations to particle positions, the plume cross-section will approach a Gaussian distribution (see e.g. Turner 1970 or Fischer *et al.* 1979). The assumption of a Gaussian plume is the most common approach to predicting concentration distribution, frequently applied with a constant and uniform dispersion coefficient defining the rate of growth of the plume cross-section. In the natural environment, however, the structure of a dispersing plume is more complex. For example, the plume centreline may not be steady, resulting in a meandering plume (see Kristensen, Jensen & Petersen 1981 for example). Additionally, the dispersion coefficient may not be constant, but instead may vary with location, or even with the plume characteristics itself (Okubo 1971).

This complexity in the environment creates a concentration field which is likely to be intermittent and highly variable. The use of a steady Gaussian plume model will certainly underpredict the intermittency of exposure, and will necessarily err in predicting either the peak concentration or the lateral extent of the plume. In this paper, we will examine the structure of a plume in the coastal ocean which is subject to both meandering of its centreline and a variable dispersion coefficient. The observations will then motivate a model framework to predict the plume dynamics. In the remainder of this introduction, we will provide background to the analysis of plume dispersion, including the structure of velocity fluctuations and their influence on plume dispersion.

It is worth noting that the term 'dispersion' in this paper is not to be confused with the shear flow dispersion theory pioneered by Taylor (1953). We use the nomenclature dispersion in this study to refer to the combined processes by which turbulence causes a plume to both meander and mix irreversibly. In addition, our use of 'turbulence dispersion' hereafter is synonymous with the commonly used term turbulent diffusion.

1.1. *Velocity fluctuations in the environment*

The primary mechanism by which a scalar cloud or plume grows is through the interaction of the scalar distribution with the ambient fluid velocities. In environmental flows, either classical three-dimensional turbulence or other flow structures, such as two-dimensional eddying motions, create fluctuating velocities which interact with the plume and disperse the scalar around its centre of mass.

Turbulence, in the strict sense, consists of three-dimensional eddies, through which the kinetic energy cascades to smaller and smaller scales until the effects of viscosity are strong enough to extinguish the velocity fluctuations (Tennekes & Lumley 1972). For steady-state conditions, the rate of transfer of energy between scales must be equal to the rate of dissipation of energy at the smallest scales. In this inertial range, the isotropic energy spectrum obeys the well-known 5/3-law of Kolmogorov:

$$E(k) = C_\epsilon \epsilon^{2/3} k^{-5/3}. \tag{1.1}$$

The dissipation rate, ϵ, or the rate of energy transfer, is independent of the scale of the eddy under consideration (see e.g. Tennekes & Lumley 1972).

If the vertical dimension is constrained by the effects of rotation or gravity, two-dimensional eddies will develop, which can be described by a streamfunction. Under an assumption of inviscid flow, the vorticity must be conserved, and will be transferred between 'turbulent' scales analogously to the kinetic energy in the three-dimensional case. Instead of using vorticity directly, Kraichnan (1967, 1971) defined the enstrophy to be one-half of the squared vorticity. Defining the rate of enstrophy transfer to be ϕ (units of T^{-3}), we follow Batchelor (1969) and Kraichnan (1967) and define the

isotropic energy spectrum to be

$$E(k) = C_\phi \phi^{2/3} k^{-3}. \tag{1.2}$$

In contrast to the three-dimensional case, where the rate of energy transfer between scales is independent of scale, in the two-dimensional case, it is the rate of enstrophy transfer (ϕ) that is independent of the lengthscale of the motions.

To generalize these results, we will define a general form for the energy density spectrum to be

$$E(k) = C_\gamma \gamma^{2/3} k^{-m}, \tag{1.3}$$

where m represents the exponential decay of the energy density versus wavenumber and would be 5/3 for the Kolmogorov spectrum or 3 for the Batchelor–Kraichnan spectrum. In this expression, γ (units of $L^{3(3-m)/2}/T^3$) represents a physical variable which is independent of the lengthscale of the motions. In three-dimensional turbulence, $\gamma = \epsilon$, the dissipation rate; while in two-dimensional turbulence, $\gamma = \phi$, the rate of enstrophy transfer. This general spectrum will be used to develop expressions for the dispersion coefficient in the next section.

1.2. *Dispersion in the environment*

As a scalar cloud disperses, its distribution is determined by the magnitude and scale of the velocity fluctuations outlined in the previous section. A meandering plume is one in which the position of the centreline is variable in space and time. The spreading of the plume around the centreline will be referred to as relative dispersion (Batchelor 1952), as it is the growth of the scalar cloud independent of its absolute position in space. Based on the scales of motion, the separation of meandering from relative dispersion can be clarified. As was stated by Sawford & Stapountzis (1986), eddies with a spatial extent larger than the plume cross-section create meandering by translating the entire plume, while eddies of scale comparable with the plume (and smaller) act to disperse the plume.

Frequently, meandering is represented as an unsteady lateral translation of the plume centreline which is independent of the spreading of the plume (Sawford & Stapountzis 1986). This is valid if there is a clear separation of scales such that those motions that define the meandering are much larger than the scale of the plume (Kristensen *et al.* 1981). If, on the other hand, the fluctuating velocities are characterized by a broad range of lengthscales, with no spectral gap to separate the 'meandering scales' from the 'dispersive scales,' then the analysis of plume growth and meandering will need to be linked.

1.2.1. *Meandering plumes*

The effects of meandering on plume structure, or on intermittency in the intensity of scalars, in the lower atmosphere has received a great deal of attention, typically through the separation of meandering and dispersive scales (Gifford 1959, 1960). In laboratory simulations, Fackrell & Robins (1982) defined intermittency, peak concentrations and probability-density functions for a plume dispersing in a turbulent boundary layer, with a focus on the differences between ground-level and elevated sources. Bara, Wilson & Zelt (1992) performed similar measurements in an open channel of water and found that the intermittency could be described well using an isotropic meandering plume model. In each of these cases, the boundary layer was neutrally stable, and the plume was developing in an unstratified turbulent boundary layer.

In the oceanic community, work on meandering plumes has focused on intermittency or, equivalently, visitation frequency. Roberts (1999) has used a statistical analysis of meandering to define a measure of intermittency downstream of a source of contamination. In the surface layer of Lake Erie, Csanady (1973) made repeated transects of a dye plume to define the instantaneous centreline of the plume and how the centreline position varied due to meandering. Based on these observations, he separated the meandering and relative dispersion using a reference frame defined around the centre-of-mass of the plume at a given downstream distance. A similar approach was taken by Stacey *et al.* (2000) to analyse a meandering coastal plume. In that study, the authors used the peak concentration as a function of distance to define the centreline concentration, thus allowing the centreline position to vary over the course of the experiment. After accounting for the meandering, Stacey *et al.* (2000) found that the plume growth was governed by a scale-dependent dispersion, which is the topic of the next subsection.

1.2.2. *Scale-dependent relative dispersion*

The growth of the plume around its centreline has received attention since the work of Richardson (1926). In general, the rate of growth of the variance of the cloud defines the local dispersion coefficient as

$$\frac{\partial \sigma_y^2}{\partial t} = 2K_y, \tag{1.4}$$

where σ_y^2 is the second moment of the lateral concentration distribution and K_y is the lateral dispersion coefficient. Frequently, the dispersion coefficient in the environment is estimated as the product of the physical lengthscale of the dispersing motions and the velocity scale of the motions (see e.g. Tennekes & Lumley 1972).

Under the assumption of a Fickian dispersion process, and for timescales long compared to the turbulent decorrelation timescale, the dispersion coefficient is a constant:

$$K_y^f \sim u_t \lambda_t, \tag{1.5}$$

where K_y^f is the Fickian dispersion coefficient and u_t and λ_t are the velocity and lengthscales of the largest motions, which typically dominate the dispersion process (Tennekes & Lumley 1972).

However, if the scale of the scalar distribution is not larger than the scale of the largest fluctuating motions, the velocity and lengthscales of the dispersive motions will vary with the plume scale. This was introduced by Richardson (1926), and later analysed by Batchelor (1952) in a general sense, and then by Okubo (1971) for the oceanic surface layer. The analysis of scale-dependent dispersion has been based on the 4/3-law (Richardson 1926; Batchelor 1952), which suggests that the dispersion coefficient depends on the plume width to the 4/3 power; or equivalently that the lengthscale of the plume would grow as $t^{3/2}$. Okubo's (1971) survey of oceanic diffusion supported the 4/3-law, as long as the analysis was applied to individual experiments. More recently, Vasholz & Crawford (1985) found that the width of a dye sheet in the open ocean grew as $t^{1.46}$, consistent with the 4/3-law.

As is described by Batchelor (1952), if the energy density of the fluctuating velocities is assumed to obey the Kolmogorov spectrum, the velocity scale, $\tilde{u}$, for motions of lengthscale $\tilde{\lambda}$, is estimated using the dissipation rate:

$$\tilde{u} \sim \epsilon^{1/3} \tilde{\lambda}^{1/3}. \tag{1.6}$$

For a plume of scale equal to $\tilde{\lambda}$, we use (1.6) to define the velocity scale of the dispersing motions, resulting in a dispersion coefficient:

$$K_y \sim \tilde{u}\tilde{\lambda} \sim \epsilon^{1/3}\tilde{\lambda}^{4/3}, \tag{1.7}$$

which is the 4/3-law introduced by Richardson (1926) for scale-dependent dispersion. Note that this result assumes that the fluctuating velocities obey the Kolmogorov inertial-range assumption for the cascade of energy to small scales.

If, on the other hand, the fluctuating velocities are more appropriately described by the two-dimensional turbulent spectrum of Batchelor (1969) and Kraichnan (1967), the velocity of motions of scale $\tilde{\lambda}$ would depend only on the rate of enstrophy transfer, ϕ, and the lengthscale. The resulting expression for the velocity scale would be

$$\tilde{u} \sim \phi^{1/3}\tilde{\lambda}. \tag{1.8}$$

Again defining the dispersion coefficient, we have

$$K_y \sim \tilde{u}\tilde{\lambda} \sim \phi^{1/3}\tilde{\lambda}^2. \tag{1.9}$$

In this case, dispersion is still scale-dependent, but now depends on the square of the lengthscale of the scalar distribution.

To generalize these results, we consider the form of the energy density spectrum given in equation (1.3). Because γ is a constant independent of the scale of the motion, the velocity scale must vary as function of only this quantity and the plume scale:

$$\tilde{u} = f(\gamma, \tilde{\lambda}). \tag{1.10}$$

Dimensional analysis then defines the scale of the fluctuating velocity for a given lengthscale $\tilde{\lambda}$ to be

$$\tilde{u} \sim \gamma^{1/3}\tilde{\lambda}^{(m-1)/2}. \tag{1.11}$$

For this general case, the dispersion coefficient becomes

$$K_y \sim \tilde{u}\tilde{\lambda} \sim \gamma^{1/3}\tilde{\lambda}^{(m+1)/2}, \tag{1.12}$$

which is a general form for the scale-dependent dispersion coefficient. Note that for $m = 5/3$, and this reproduces the 4/3-law and for $m = 3$, and the dispersion depends on the scale-squared.

1.2.3. *Fluctuating plume dynamics*

In the atmospheric literature, a fluctuating plume model is frequently applied to model the near-field concentration structure (Gifford 1959, 1960). In this model, the motion of the centreline and the growth of the plume around the centreline are assumed independent and uncorrelated. If such independence exists, then the dispersion of the plume can be separated into meandering and relative components which would be linearly superposed. This topic is taken up again in § 4.2 for the study at hand, but the limitations of this approach merit some discussion here.

At a particular location downstream of the source, velocity fluctuations with lengthscales larger than the plume will cause the plume to meander, while those with lengthscales comparable with the plume size will dominate the dispersion of the plume. In the near field, these two processes are likely to be governed by separate velocity structures: the meanders will be dominated by the large two-dimensional structures and the dispersion by the three-dimensional turbulence field. This distinction justifies

the usual fluctuating plume approach, which separates the meander and dispersion components.

The discussion of the previous subsection, however, suggests that if the plume is of lateral scale comparable to the two-dimensional motions, then those motions will become dispersive, with a scale-squared dispersion law. In this scenario, the meander and the dispersion around the centreline are both determined by the same set of velocity structures and the usual assumption of independent, uncorrelated motions may not be valid. As a result, we expect there to be a transition from a fluctuating separable plume to a scale-squared dispersion law at some intermediate distance from the plume source, determined by the point at which the plume scale is comparable to the large two-dimensional motions.

1.3. *Outline of the paper*

This study examines the meandering and dispersion of a plume in the coastal ocean using a dye plume dataset collected using a state-of-the-art autonomous underwater vehicle (AUV) in a near-coastal flow environment.

The paper is organized as follows. In § 2, the field site and instrumentation used to collect the data are described. The measurements and data are presented in § 3. Plume meandering is analysed in § 4, and a simple model for quantifying meandering is suggested. Section 5 contains an analysis of scale-dependent dispersion for the dye plume dataset, followed in § 6 by a discussion of how it compares with the theory discussed above. The results are summarized in § 7.

2. Experiment and instrumentation

The experiment was performed in the near-coastal zone at the Army Corps of Engineers Field Research Facility at Duck, North Carolina. The study site was located over 700 m offshore, well outside the surf zone, within the nearshore region (see Lentz 1995; Austin 2002) where the bottom slopes gently offshore (figure 1). The measurements presented in this paper were conducted on May 16, 2001.

For this study, a mixture of Rhodamine WT dye, released at a rate of $3\,\mathrm{g\,min^{-1}}$, was mixed with the ambient sea-water and released from a near-bed source. In order to minimize the effects of turbulence generated from the source itself, the source consisted of soaker hose tubing wrapped around an open meshed cylinder with the dimensions of a 55 gallon drum (approximately 0.91 m high and 0.61 m in diameter). The result was a zero-buoyancy diffuse source of dye near the bed with minimal momentum. A filter system was incorporated to minimize the potential for clogging and ensure that the flow rate and concentrations at the source were constant in time.

A 600 kHz Broadband Workhorse acoustic Doppler current profiler (ADCP) (RD Instruments, Inc.) was deployed within a few metres of the source in an upward-looking configuration. The ADCP recorded velocities in 0.5 m bins, the first of which was located 1.25 m above the bottom. An OS200 (Ocean Sensors, Inc.) conductivity, temperature and depth profiler (CTD) was used to measure profiles of temperature and conductivity as a function of pressure, approximately once per hour. From these variables, the density and stratification were computed.

The dye concentration measurements were made using an autonomous underwater vehicle (AUV) called REMUS (Woods Hole Oceanographic Institution/Hydroid, Inc.). With the accurate placement of two acoustic transponders deployed at known locations, and a combination of long-baseline and ultra-short-baseline navigation and dead reckoning via a downward looking 1200 kHz ADCP, REMUS

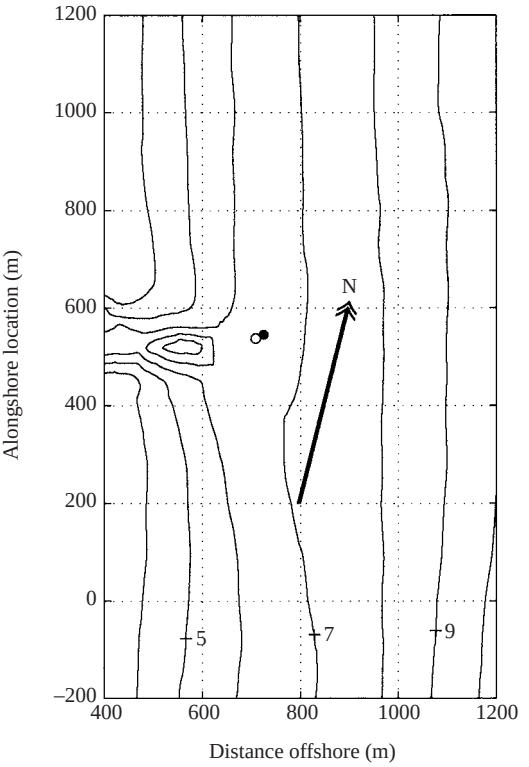

FIGURE 1. Bathymetry offshore of Field Research Facility, Duck, NC. The open circle indicates the location of an upward-looking ADCP. The bold dot indicates the dye source location. Isobaths are contoured in 1 m intervals.

is capable of following its programmed path to an accuracy better than 2 m in the horizontal. Unfortunately, for this experiment, there were problems in the the acoustic transponders placement, resulting in uncertainties of up to 10 m in the absolute horizontal vehicle location.

In the vertical direction, using its ADCP as an altimeter, the AUV can maintain its programmed altitude to within 0.10 m. REMUS was also equipped with a fluorometer (Seapoint, Inc.), sampling the water at a frequency of 9 Hz. With the AUV executing its programmed path at a nominal speed of 1.5 m s^{-1}, the horizontal resolution for dye concentrations was approximately 0.15 m. The fluorometer was operated in a fixed range such that it could reliably detect dye concentrations as low as 0.02 parts per billion (p.p.b.).

The dye concentration measurements made by REMUS were designed to capture both the spatial and temporal variability of the plume. REMUS was first programmed to measure the dye concentrations along a transect which crossed the plume approximately 150 m downstream from the source at a height of 1.5 m above the bottom. (Mission 1, shown in figure 2*a*) This measurement path was repeated thirty-nine times and provided a means of assessing both the lateral and temporal variability in the plume's structure. Second, REMUS was programmed to subsequently measure the larger-scale plume structure at distances up to 1200 m downstream from the source (Mission 2, shown in figures 2*b* and 2*c*). This measurement path (also at an altitude of 1.5 m) was chosen to capture both the lateral and longitudinal spatial characteristics

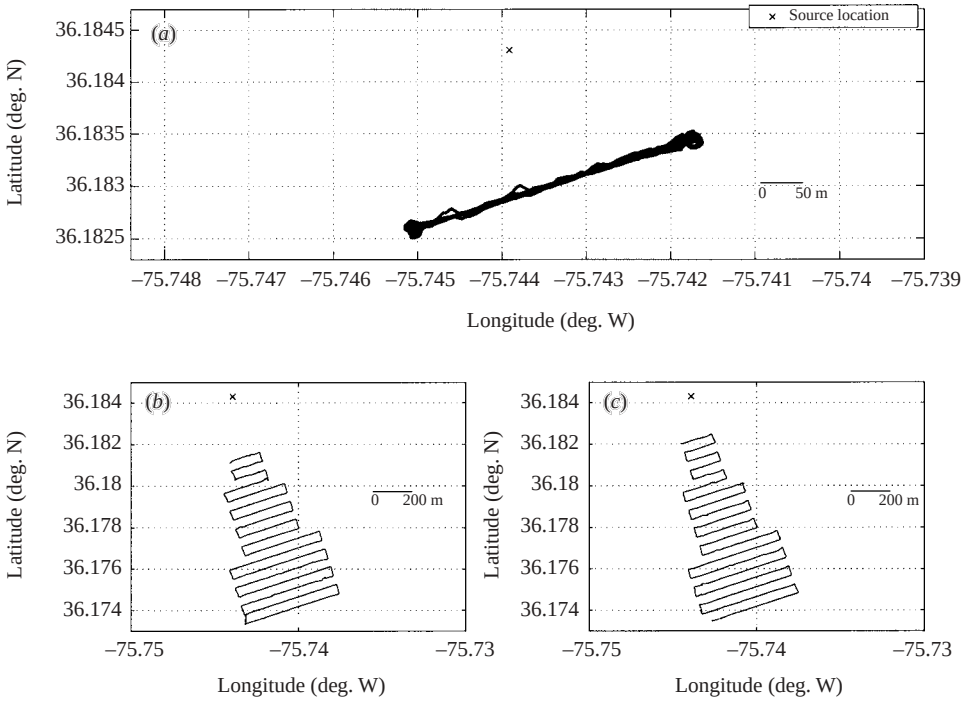

FIGURE 2. AUV flight path. (*a*) Mission 1: 39 consecutive transects 150 m downstream from the dye source. (*b*) Mission 2, outbound leg: transects spaced at 50 m intervals downstream from the source. (*c*) Mission 2, inbound leg: transects spaced at 50 m intervals downstream from the source. Source location denoted by ×.

of the plume that developed downstream of the source, and was performed twice in succession (hereafter, referred to as the inbound and outbound legs of Mission 2).

The fluorometer on REMUS was calibrated using standards prepared with local seawater for dilution to ensure that the effects of turbidity were included. Calibrations included additional emphasis on the lower concentration range to better define the low signal-to-noise measurements expected long distances from the source.

3. Measurements

The focus of this paper is on a plume created on May 16, 2001, with the dye release starting at 13:05 (UTC). The plume was allowed to develop for an hour before the AUV was deployed to start Mission 1 (the repeated transects). The dye was continually released until the completion of Mission 2 (approximately 19:00 UTC). Based on the average near-bottom velocities measured by the ADCP (see below), the source concentration was approximately 540 p.p.b. (assuming an effective source area of $\sim 0.55\,\mathrm{m}^2$).

3.1. *Wind measurements*

Wind velocity and direction were collected at station DUCN7, which was located near the dye release at the end of an adjacent pier. This station is owned and maintained by the National Data Buoy Center. Wind speed and direction were averaged over ten minute periods. Using the quadratic drag law of Large & Pond (1981) these records were then used to compute cross- and alongshore components of wind stress shown

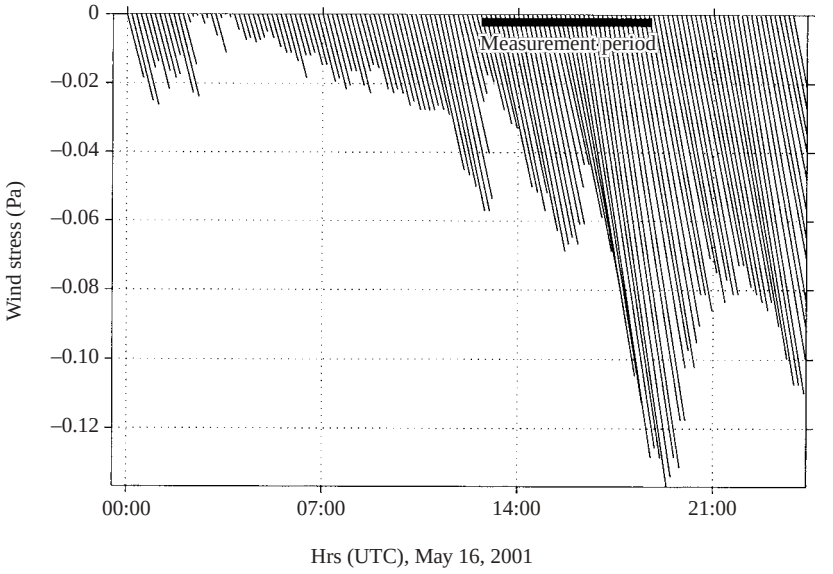

FIGURE 3. DUCN7 wind record. Wind stress (Large & Pond 1981) observations for May 16, 2001. Vertical vectors indicate winds parallel to the coast.

in figure 3. For the duration of May 16, the winds are predominantly downwelling favourable (from the north-northwest, or roughly parallel to the shore) with the amplitude increasing throughout the day, with a large increase occurring around 15:25 UTC.

3.2. *Stratification observations*

Temperature and salinity, as functions of pressure (depth), were collected on an approximately hourly basis starting at 11:17. These data were used to compute density, block-averaged to a 0.25 m grid for each profile, and converted to a height above bottom coordinate system using the local depth (comparable to the local depth at the source) (figure 4). The first cast, taken approximately 90 minutes prior to the initial dye release indicates a 2 m high bottom mixed layer, capped by a pycnocline. Above the pycnocline is a 4 m thick surface mixed layer. As the day progresses, the surface mixed layer deepens, and as a result, both the pycnocline and bottom mixed layer are reduced in extent. By the time REMUS made its first concentration measurements, the bottom mixed layer is about 1.5 m thick with a pycnocline extending to about 2 m above the bottom.

It appears that the temporal variability in the surface and bottom mixed layers observed is not necessarily due to shear instability and mixing processes. In fact, using the ADCP data presented below, one finds that the gradient Richardson number is large in the pycnocline for all casts prior to 16:06. It is more likely that what is observed in figure 4 is explained by advective processes. Under downwelling favourable wind conditions, an offshore velocity in the bottom boundary layer is expected which would cause the pycnocline to migrate to a deeper isobath.

The bottom mixed layer continues to thin in time as the surface mixed layer deepens. By 16:06, the water column is nearly homogeneous with no appreciable bottom mixed layer. The last two profiles show a thin bottom mixed layer (1–2 m), capped by a relatively weak pycnocline.

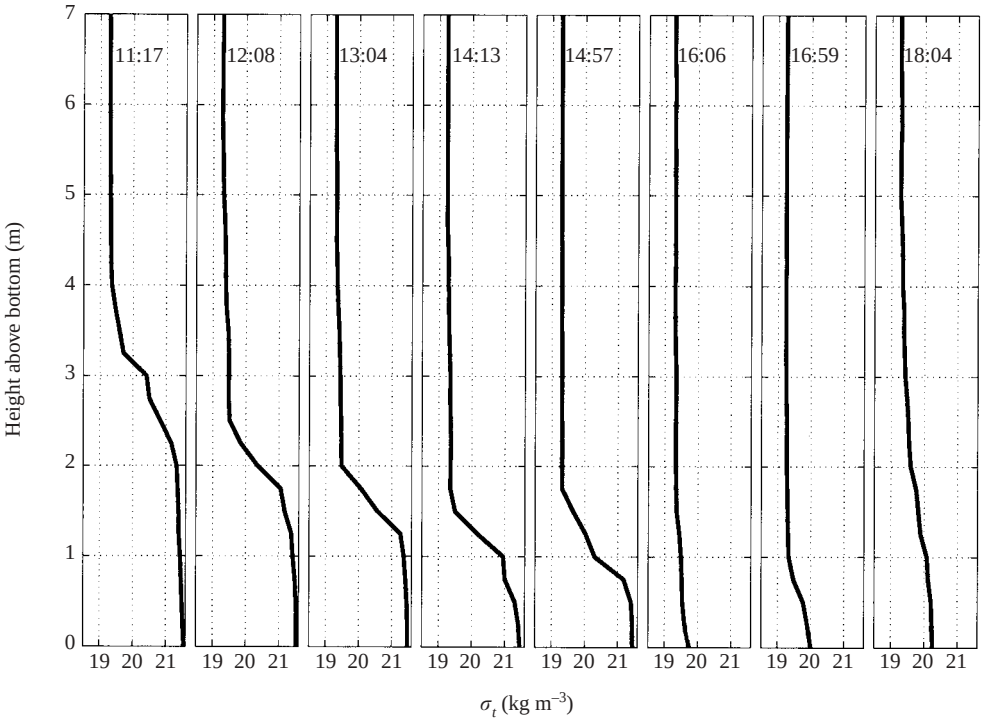

FIGURE 4. Density profiles for May 16, 2001 from FRF pier. Profiles are normalized into a height above bottom coordinate system. (All times given at the top are in UTC).

3.3. *Current observations*

The dominant flow pattern during this period was a south-southeastward current that was predominantly along-isobath. The ADCP record (figure 5) exhibits changes in vertical structure over the course of the study. The slow intensification of the current is attributable to the north-northwesterly winds (figure 3) which drive a significant downcoast and downwind surface current. While the dominant flow direction is along-isobath (figure 5*b*), there is a significant cross-isobath flow (figure 5*a*) present throughout the study which exhibits temporal variability. These fluctuations will be characterized when the plume meandering is addressed in § 4.

3.4. *Dye concentration fields*

As discussed earlier, the study consisted of two separate missions performed by REMUS. Each mission's dye concentration time series are discussed separately below.

3.4.1. *Mission 1*

The first mission involved repeatedly measuring the dye concentration at an altitude of 1.5 m above the bottom at a transect 150 m downstream from the dye source. A time series of the dye concentration measured with the REMUS fluorometer during this mission is shown in figure 6(*a*). The time series is characterized by 39 distinct peaks of measurable dye during each transect. A notable feature of the time series is the dramatic increase in peak dye concentration from 15:30 onward. This behaviour

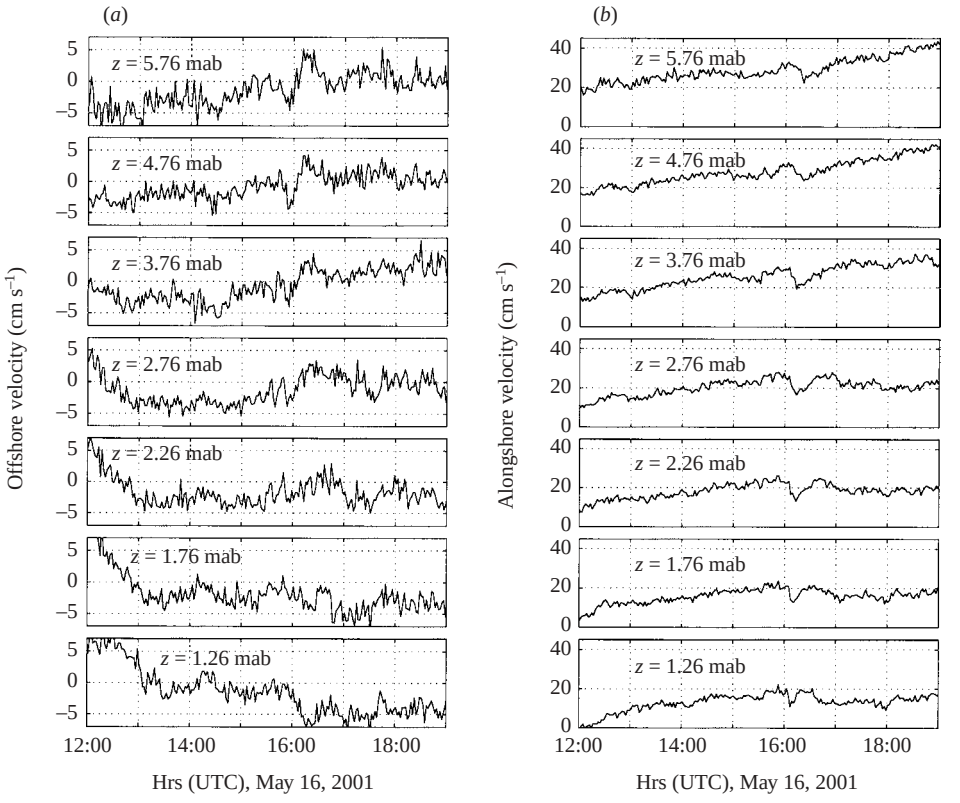

FIGURE 5. Two-minute averaged ADCP record (in cm s^{-1}). (*a*) Offshore velocity, (*b*) alongshore velocity (positive in direction of Kelvin wave propagation). Note: scales are different for offshore and alongshore velocity components.

is readily explained by the CTD profiles shown in figure 4: the CTD profiles taken at 14:13 and 14:57 describe a very thin bottom mixed layer capped by a pycnocline at 1.5–2 m. Since the AUV is measuring dye concentrations at an altitude of 1.5 m above the bottom, it is only measuring dye within the pycnocline. Consistent with the expectation that stratification should limit the vertical migration of the dye (see e.g. Turner 1973), the AUV is only measuring trace concentrations of dye. This is consistent with the few available dye profiles measured during the experiment. These profiles (not shown) show a dye plume confined to 1.5–2 m above the bottom. The vertical concentration is nearly uniform with a rapid decrease in concentration near the pycnocline. For the later transects of Mission 1, however, the stratification defining the top of the bottom mixed layer is significantly weakened (as suggested by the density profile at 16:06), and the dye mixes more thoroughly through the lower layer. The elevated dye concentrations measured after 15:30 suggest that the REMUS's fluorometer is measuring dye in a more well-mixed water column, in contrast with measuring low concentrations at the top of the pycnocline earlier during Mission 1. The disappearance of the bottom mixed layer for times after 15:30 is also evident in the acoustic backscatter record from the ADCP (not shown).

Using navigation data stored by the AUV, the time series of dye concentration can be converted into dye concentrations as a function of horizontal position (longitude and latitude) and subdivided into thirty-nine individual transects. One example transect

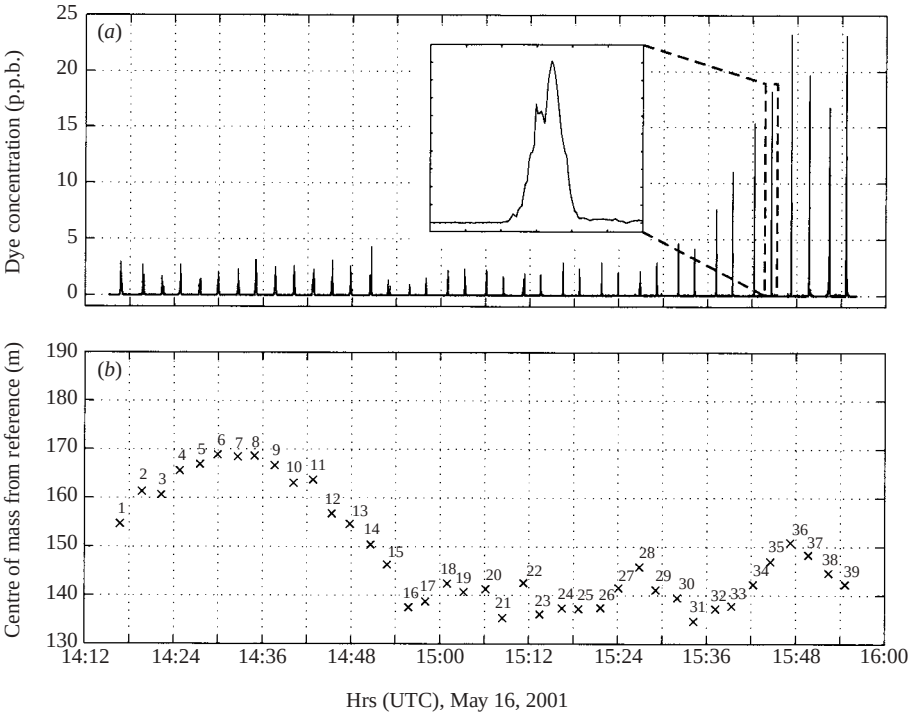

FIGURE 6. Mission 1 time series. (*a*) Dye concentration in p.p.b. (inset plot shows dye distribution for transect #35). (*b*) Position of centre of mass.

is shown in the inset of figure 6(*a*). Once normalized onto a consistent coordinate system defined by a fixed reference location, the position of the centre of mass of each transect, $\overline{y}$, can be computed (figure 6*b*) using the following expression:

$$\overline{y} = \frac{\int_{y=0}^{y=L} C(y) y \, \mathrm{d}y}{\int_{y=0}^{y=L} C(y) \, \mathrm{d}y}, \tag{3.1}$$

where $y = 0$ is defined by a fixed point of reference. The significant variability in lateral plume position during Mission 1 is suggestive of a meandering process, which will be explored in detail in the next section.

Similarly, one can use the second moment of the concentration distributions to infer a lengthscale for the width of the plume as a function of time:

$$\tilde{y} = \sqrt{\frac{\int (y - \overline{y})^2 C(y - \overline{y}) \, \mathrm{d}y}{\int C(y) \, \mathrm{d}y}}. \tag{3.2}$$

This lengthscale is useful for inferring the lateral dispersion and quantifying the effects of meandering on measured dispersion. These issues will be explored in § 4.

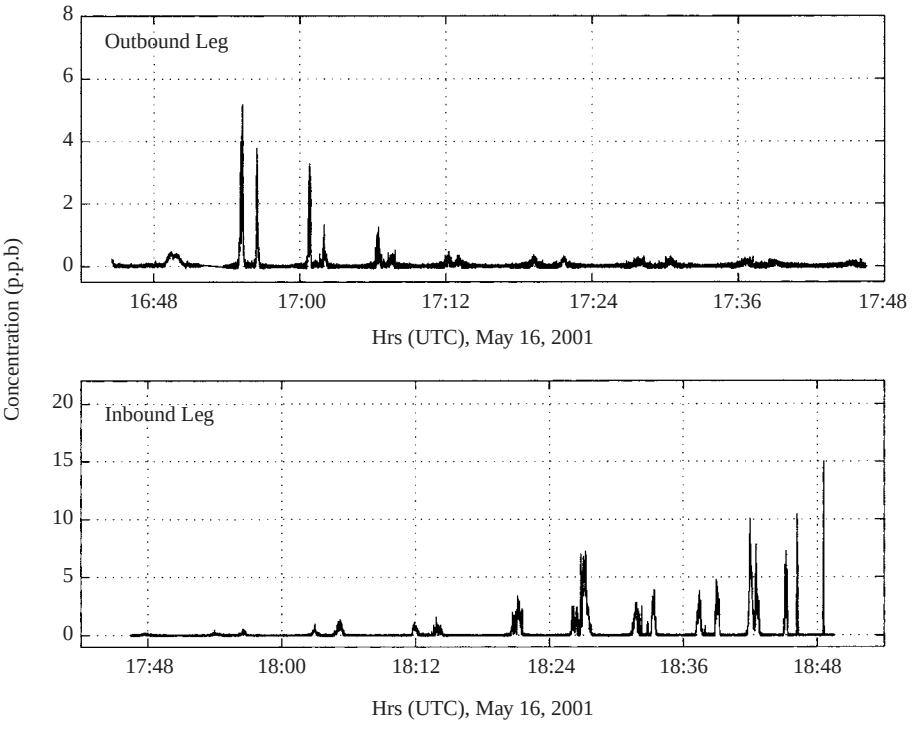

FIGURE 7. Mission 2 dye concentration time series (in p.p.b.). Note: different scales for inbound and outbound legs due to inbound leg reaching points nearer the source.

3.4.2. *Mission 2*

As previously mentioned, the second mission involved dye measurements over a large survey area at distances up to 1.2 km from the source. The time series of dye for both the inbound and outbound legs of this mission are shown in figure 7.

Dye concentrations span several orders of magnitude during the course of the mission. Peak concentrations for transects near the source for the outbound leg are near 5 p.p.b., in contrast to peak concentrations of 15 p.p.b. for the near-source transects for the inbound leg. This disparity is largely explained by the inbound leg including a few transects nearer to the source than the outbound leg (see figure 2). Although difficult to resolve with the naked eye in figure 7, significant dye concentrations relative to the fluorometer's noise floor (0.02 p.p.b.) are detected at the transect furthest from the source ($\sim$ 17:45 UTC).

The time series shown in figure 7 can be converted into dye concentrations as a function of horizontal position using the navigation data recorded by the AUV. This spatial dye distribution is used to analyse the scale-dependent dispersion discussed in § 5.

4. Plume meandering

The centre-of-mass position is quite variable, as is evidenced by the cross-shore excursions shown in figure 6(*b*), indicative of a meandering plume. This behaviour is not surprising since the cross-shore velocities also exhibit significant temporal variability.

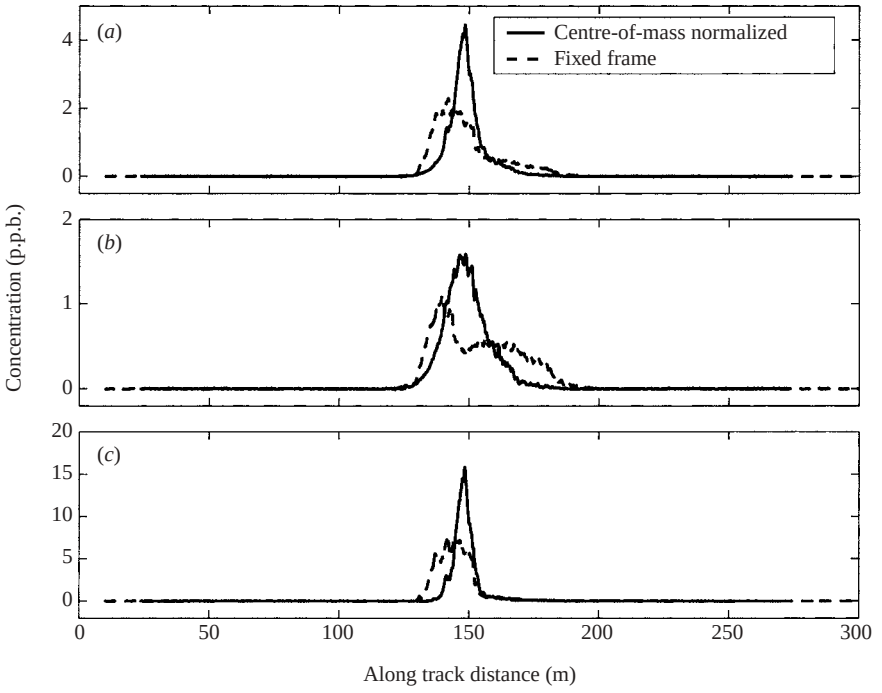

FIGURE 8. Mean concentration profiles (in p.p.b.). (*a*) All transects, (*b*) transects 1–31, (*c*) transects 32–39.

4.1. *Effect of meandering on dispersion*

It is important to understand the role meandering plays in the effective dispersion of the plume. Using a set of observations of dye concentrations in Lake Huron, Csanady (1973) noted that the position of the centre of mass of each individual concentration profile changed over the course of the measured runs. Because of this behaviour, he suggested that the mean distribution, as calculated in a fixed reference frame, would be several times wider than any individual profile, and furthermore, that the peak of the mean profile would be significantly less than any instantaneously measured peak concentrations. Csanady concluded that in order to remove the effect of the motion of the concentration profiles temporally, the mean profile should be computed using a moving reference frame, i.e. one with respect to the temporally changing centre-of-mass position. By computing the mean with respect to this reference frame, he found that the centre-of-mass averaged profile came much closer to replicating the width and peak concentrations observed for any instantaneous profile than the fixed-frame average.

These two different mean concentration profiles are plotted for the 39 transects in figure 8. Figure 8 shows mean profiles based on the first 31 transects, the last eight transects, and all 39 transects. The data are presented in this fashion in order to distinguish between periods of differential vertical mixing, as was suggested by the change in profile amplitudes at 15:30 noted previously.

Consistent with Csanady's (1973) findings, the centre-of-mass averaged profiles have a much larger peak concentration than the fixed frame mean profiles. In addition, the mean plume is narrower for the centre-of-mass calculation. It should be noted that the fixed-frame profiles shown in figure 8(*b*) have a bimodal distribution. This

Transects	$\overline{y}$ (m)	$\tilde{y}_{fix}$ (m)	$\tilde{y}_{cm}$ (m)	σ^2_{cm} (m^2)
1–39	148.7	12.7	8.6	119
1–31	150.3	14.3	8.7	130
32–39	145.8	8.9	8.4	24

TABLE 1. Mean concentration profile characteristics. Variables are defined in the text.

behaviour is attributable to the meandering of the plume, for which the data set only has 2–3 realizations of meander events.

The plume-width lengthscales can be quantified by equation (3.2) and are summarized in table 1. In spite of the differences in peak concentration during the experiment, all three centre-of-mass lateral scales, $\tilde{y}_{cm}$ are ~ 8.5 m. In contrast, the fixed-frame scales $\tilde{y}_{fix}$ range from 8.9 to 14.3 m, depending on the transects over which the dye distribution is averaged. This is to be expected based on the time series of the centre-of-mass position (figure 6*b*): the cross-shore current variability, and hence the plume meandering, is reduced towards the end of Mission 1. The consequences of including or removing the effects of meandering are significant when estimating the lateral turbulent dispersion. For the early plume transects (1–31), the fixed-frame lengthscale is 63% higher than the moving-frame estimate, which suggests a bulk dispersion coefficient in the fixed frame that is more than 2.5 times larger than in the moving frame. In the next subsection, dispersion coefficients for meandering and dispersion around the centreline will be defined explicitly.

4.2. *Decomposing mean dispersion*

An examination of the meandering plume models described in § 1.2.1 motivates a decomposition of the mean plume dispersion into individual components associated with turbulent dispersion and meandering, associated with larger-scale velocity fluctuations. Of particular note is the linear separation of the meander and relative dispersion components by Sawford & Stapountzis (1986), which found that such a decomposition was appropriate in the near field of plumes developing within a stably stratified atmosphere.

Following Csanady (1973), the off-axis plume displacement of an individual parcel of marked fluid can be written as

$$y(t) = \int_0^t v' \, \mathrm{d}t_1, \tag{4.1}$$

where $v' = v'(t)$ is defined as the velocity component perpendicular to the main plume axis. If this velocity component is decomposed into meandering and turbulent components, i.e.

$$v' = v_m + v_t,$$

the square of the position of the fluid parcel becomes

$$y^2(t) = \int_0^t \int_0^t \left(v_m^2 + 2v_m v_t + v_t^2\right) \mathrm{d}t_1 \, \mathrm{d}t_2. \tag{4.2}$$

To define the lateral scale of the plume, we take the mean value of equation (4.2) over a large number of particles (or, equivalently, an ensemble average, see

Fischer *et al.* 1979, for example), which yields

$$\overline{y^2(t)} = \int_0^t \int_0^t \left(\overline{v_m^2} + \overline{2v_m v_t} + \overline{v_t^2}\right) \mathrm{d}t_1 \, \mathrm{d}t_2. \tag{4.3}$$

However, if the turbulent and meandering velocities are assumed independent and uncorrelated, then the second term on the right-hand side of (4.3) vanishes leaving

$$\overline{y^2(t)} = \int_0^t \int_0^t \overline{v_m^2} \, \mathrm{d}t_1 \, \mathrm{d}t_2 + \int_0^t \int_0^t \overline{v_t^2} \, \mathrm{d}t_1 \, \mathrm{d}t_2. \tag{4.4}$$

The assumption of independent and uncorrelated meandering and turbulent motions merits further discussion. Meandering will be dominated by those motions larger than the plume dimension whereas dispersion will be set by motions of scale similar to the plume itself. The separation into two independent dispersion coefficients therefore depends on a scale separation between those velocity components causing meandering and those creating dispersion. Because meandering will be dominated by the large-scale motions, we would expect that such a decomposition would be valid in the near field, but would probably break down as the plume grows to a scale comparable to the larger-scale motions driving meandering. This is consistent with results in the atmospheric literature (e.g. Sawford & Stapountzis 1986), where a fluctuating plume model, which separates the meandering and relative dispersion components in the same way, is found to be applicable in the near field. As we will see in § 5, it appears that this linear decomposition is valid to a downstream distance of about 700–800 m.

Equation (4.4) describes a model where the lateral plume scale can be linearly separated into two components: one due to meandering (v_m) and one due to the turbulent velocities (v_t). Taking the time derivative of each side, we have

$$\frac{\partial}{\partial t}(\overline{y^2(t)}) = \frac{\partial}{\partial t}\left(\int_0^t \int_0^t \overline{v_m^2} \, \mathrm{d}t_1 \, \mathrm{d}t_2\right) + \frac{\partial}{\partial t}\left(\int_0^t \int_0^t \overline{v_t^2} \, \mathrm{d}t_1 \, \mathrm{d}t_2\right). \tag{4.5}$$

Each of the terms on the right-hand side represents a dispersive process, and, by the definition of the dispersion coefficient (equation (1.4)), can be related to a dispersion coefficient

$$\frac{\partial}{\partial t}(\overline{y^2(t)}) = 2K_m + 2K_t \tag{4.6}$$

or

$$K_{tot} = K_m + K_t, \tag{4.7}$$

where K_{tot} is the total effective dispersion and K_m and K_t are the dispersion coefficients attributable to the processes of meandering and turbulent lateral dispersion, respectively. This simple analysis illustrates that the total effective dispersion is a simple superposition of the meandering and turbulent processes, assuming meandering and turbulent motions are independent and uncorrelated.

If the components of dispersion are additive as suggested by the simple analysis above, the lateral plume lengthscale attributable to turbulent dispersion can be estimated by

$$\sigma_t^2 = \tilde{y}_{fix}^2 - \sigma_{cm}^2, \tag{4.8}$$

where $\tilde{y}_{fix}$ is the lateral scale of the plume in the fixed reference frame (table 1) and σ_{cm} is the lateral scale of motion for the centre of mass. For transects 1–31, the variance in the centre-of-mass position is $\sigma_{cm}^2 = 130\,\mathrm{m}^2$ (see table 1). Substituting this variance into (4.8) along with the value for $\tilde{y}_{fix}$ from table 1 yields $\sigma_t^2 = 72\,\mathrm{m}^2$ or $\sigma_t = 8.5\,\mathrm{m}$, comparable to the value of $\tilde{y}_{cm} = 8.7\,\mathrm{m}$ shown in table 1.

By integration of equation (1.4), the Fickian dispersion coefficient can be calculated directly from the observed lengthscales presented in table 1. To be clear, the Fickian (constant) dispersion coefficient can be calculated based on observations of $\tilde{y}$ (the lateral scale of the plume) as

$$K_y^f = \frac{(\tilde{y}_x^2 - \tilde{y}_0^2)}{(2x/U)}, \tag{4.9}$$

where $\tilde{y}_x$ is the plume scale at a distance x downstream of the source, $\tilde{y}_0$ is the plume source width at $x = 0$, and U is the mean advective velocity. For Mission 1 (crossings 1–31), $x = 150$ m, $U = 0.17\,\mathrm{m\,s^{-1}}$, $\tilde{y}_0 = 0.18$ m (assuming the source to be a uniform concentration of width 0.61 m, such that $\tilde{y}_0 = 0.61/\sqrt{12}$) and $\tilde{y}_x$ is given in table 1. In the fixed reference frame, a lateral scale of 14.2 m defines a total dispersion coefficient using equation (4.9) of $K_{tot} = 0.1142\,\mathrm{m^2\,s^{-1}}$. In the moving reference frame, the lateral plume scale is 8.7 m, which implies a relative (or centreline) dispersion of $K_t = 0.0429\,\mathrm{m^2\,s^{-1}}$. Using the linear superposition defined by equation (4.7), this implies a meander dispersion coefficient, $K_m = 0.0714\,\mathrm{m^2\,s^{-1}}$, approximately 1.7 times the relative dispersion around the centreline. How this value compares with the magnitude of the relative dispersion coefficient when spatial variability in dispersion is accounted for is discussed in § 6.2. In the next subsection, we present a model of the meandering process based on a time series of velocity measurements.

4.3. *A simple model of plume meandering*

One simple model of the meandering of the dye plume is to assume that the meandering observed can be explained by a spatially uniform velocity field with its temporal variability defined by the single-point velocity measurements of the ADCP near the source. If we assume that the measured velocities at the source are representative of the velocities nearby (up to 150 m downstream), we can construct pathlines for individual parcels of dye that are released from the source,

$$\boldsymbol{x}_i(t + \Delta t) = \boldsymbol{x}_i(t) + \boldsymbol{u}(t)\Delta t, \tag{4.10}$$

where $\boldsymbol{x}_i$ is the location of an individual parcel of dye at time t which was released at time t_i (i.e. $\boldsymbol{x}_i(t_i) = (0, 0)$, with $(0, 0)$ being the source location), $\boldsymbol{u}$ is the velocity measured by the ADCP at time t, and Δt is the time-step discretization. These pathlines represent the path of an individual parcel of dye released from the source.

From these pathlines, we then define streaklines by noting the location of all the parcels (that have been previously released from the source) at a particular time t:

$$\boldsymbol{X}(t) = (\boldsymbol{x}_1(t), \boldsymbol{x}_2(t), \boldsymbol{x}_3(t), \ldots). \tag{4.11}$$

The streaklines represent snapshots of the plume centreline (in the absence of any diffusive/dispersive processes) and represent a model of the plume centreline sampled in the field.

The cross-shore location of the streakline at a distance 150 m downstream from the source is compared with the centre of mass of the AUV measured dye profiles in figure 9. To first order, the agreement is very good. The streakline analysis reproduces the qualitative on- and offshore motion of the plume noted in the centre-of-mass calculations. The two curves appear offset by approximately 10 m. This offset can easily be explained by a small ADCP compass error ($O(1$–$2^\circ)$), local changes in bathymetry, spatial variations in the velocity field, or, as noted in § 2, issues related to the transponder deployment. One might postulate that the differences between the two curves is attributable to Stokes drift (see Stokes 1847); however, simple scaling of

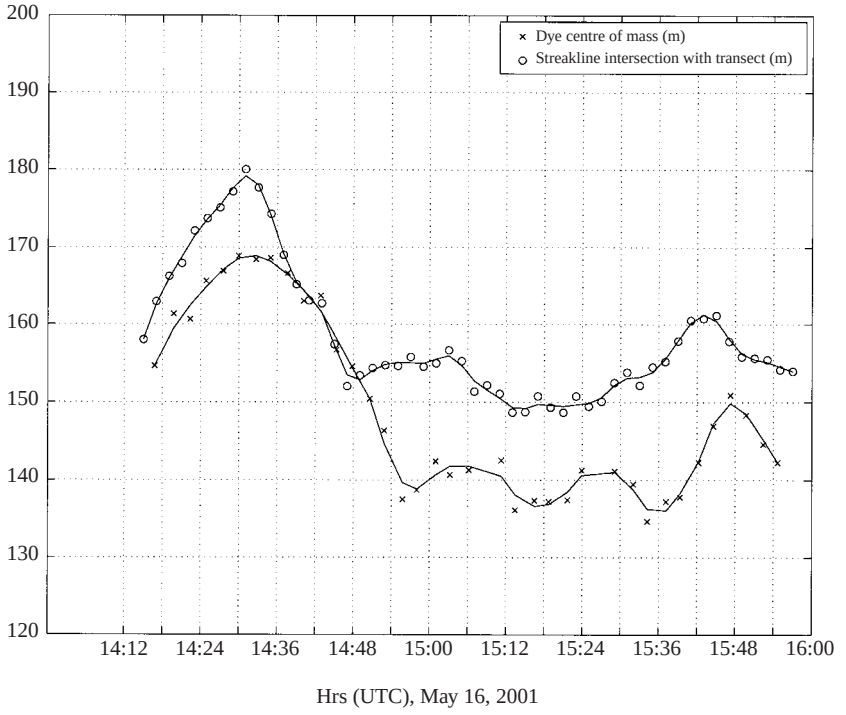

FIGURE 9. Streakline comparison. Plume meandering (based on dye concentrations) and streakline motion 150 m from the source are compared plotted as functions of time. Data points are shown with symbols. Plotted lines are based on 8 minute low-pass filtered data sets.

the effective Stokes drift (using wave height gauges monitored at the Field Research Facility) show that advection by Stokes drift should be negligible during the time period of this study.

One might also consider using the fixed ADCP streaklines to estimate the dispersive effect due to meandering. For transects 1–31, the variance in streakline position $\sigma^2_{s-cm} = 95\,\mathrm{m}^2$, which is slightly less than the measured $\sigma^2_{cm} = 130\ \mathrm{m}^2$, so the dispersion coefficient due to meandering would be underpredicted by this simple model by about 25%. The reduction in variability of the flow is to be expected in this type of model due to the neglect of spatial variations in the flow. The fact that 75% of the dispersion can be accounted from using a uniform velocity field suggests that the motions dominating meandering are of very large scale and reinforces the use of this simple approach to quickly estimate the scale of meandering dispersion. One would expect the quantitative aspects of meandering-induced apparent diffusion to be dependent on the hydrodynamic conditions at a particular time and location. Nonetheless, it appears promising that a uniform, but unsteady, velocity field can accurately predict this important contributor to the overall dispersion.

5. Scale-dependent dispersion

The scale-dependent lateral dispersion is next estimated using two different analytic methods. First, an analytic solution to the advection–diffusion equation, a slightly modified form of that derived by Brooks (1960) and Stacey *et al.* (2000) (hereafter referred to as ST2K), is used to find the scale-dependent lateral dispersion coefficient.

This method makes use of the centreline concentrations at different radial distances from the source. Second, using the lateral plume lengthscale (as defined by the square root of the second moment) as a function of distance from the source and the definition of the dispersion coefficient as given by (1.4), the scale-dependent dispersion is estimated. Finally, a compound fit to account for the physical structure of the flow is considered.

5.1. *Analytic solution to the advection–diffusion equation*

Following ST2K, the effects of the plume meandering are removed from the dispersion by relying on the peak or centreline concentration measurements as a function of downstream distance from the source. This approach 'straightens out' the meandering plume, and allows analysis in a reference frame aligned with the plume axis. The mathematics which follows is only a brief outline of the solution presented by ST2K. The reader is directed to that paper for the details of the derivation.

If the centreline plume axis is defined as the x-axis, the governing equation for the steady-state dye concentration distribution is expressed by

$$U\frac{\partial C}{\partial x} = \frac{\partial}{\partial x}\left(K_x\frac{\partial C}{\partial x}\right) + \frac{\partial}{\partial y}\left(K_y\frac{\partial C}{\partial y}\right) + \frac{\partial}{\partial z}\left(K_z\frac{\partial C}{\partial z}\right), \tag{5.1}$$

where U is the mean along-plume axis velocity. As suggested in § 1, we expect scale-dependent dispersion to be relevant; hence, we define the lateral dispersion coefficient K_y by the expression

$$\frac{K_y}{\epsilon_0} = \left(\frac{L}{b}\right)^n = f(x), \tag{5.2}$$

where b is the initial plume width (the source width), L is the lateral scale of the plume, ϵ_0 is a constant of proportionality, and $f(x)$ defines the downstream variability of K_y. In this expression, n is the exponent that defines the scale-dependence of the dispersion. Referring to the discussion of § 1.2.2, specifically equation (1.12), we see that $n = (m+1)/2$, where m is the exponent in the energy spectrum. In the three-dimensional turbulent inertial range, $n = 4/3$, which is the 4/3-law of Richardson (1926), Batchelor (1952) and Okubo (1971). For two-dimensional turbulence, $n = 2$, or a scale-squared law, is expected.

In the subsequent analysis, the influence of longitudinal dispersion is neglected, assuming advection dominates in that direction. As in ST2K, the analysis which follows allows a general result where n is not necessarily the constant $n = 0$ (Fickian turbulent diffusion), $n = 1$, or $n = 4/3$ (Brooks 1960; Stommel 1949). In contrast to ST2K, however, we will allow n to be a tunable parameter in the least-squares best fit to our analytic solution presented below.

Ignoring the vertical direction and focusing on the lateral spread of the plume, it can be shown that (see ST2K) the centreline solution (at $y = 0$) to

$$U\frac{\partial C}{\partial x} = K_y\frac{\partial^2 C}{\partial y^2} \tag{5.3}$$

for a source of width b centred at $y = 0$ for $n \neq 2$ (the special case of $n = 2$ will be considered later in § 5.3) is

$$C_h(x,0) = C_0\ \mathrm{erf}\left(\left[\tfrac{2}{3}\left[(2-n)\beta x/b + 1\right]^{2/(2-n)} - 1\right)\right]^{-1/2}\Big), \tag{5.4}$$

where C_h is the concentration distribution attributable to only horizontal dispersion

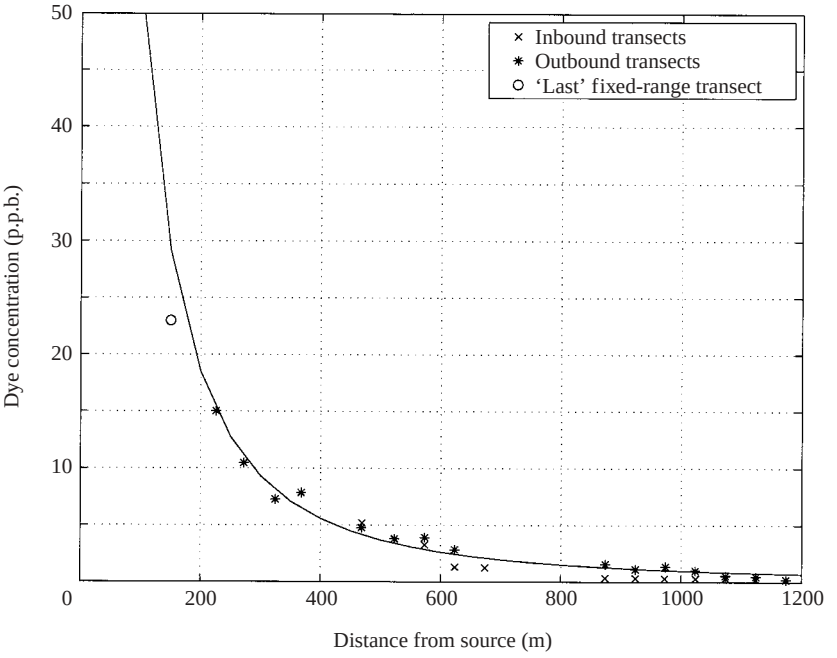

FIGURE 10. Analytic model fit versus centreline concentration data. Data from Mission 2 are shown along with the final transect of Mission 1 ($x = 150$ m).

and $\beta = 12\epsilon_0/Ub$. Note that in terms of β, the dispersion coefficient can be written as $K_y = \beta(Ub/12)(1/b^n)L^n$.

Assuming a uniform vertical diffusion coefficient, estimated as $O(10^{-5})\,\mathrm{m^2\,s^{-1}}$ using a mean current of $0.17\,\mathrm{m\,s^{-1}}$, a bottom mixed layer of 2 m, and friction velocity estimates previously measured at Duck (e.g. Lentz 2001), it can be shown that the dye should be well-mixed over the entire bottom mixed layer about 60 m downstream of the source. Therefore, for $x > 60$ m the vertical dispersion component can be represented by a dilution based on the ratio of the source height to the mixed layer height, H. The solution for the peak centreline concentration (for $n \neq 2$) is given by

$$C_{CL}(x) = C_0 \frac{h}{H}\ \mathrm{erf}\Big(\big[\tfrac{2}{3}\big([(2-n)\beta x/b + 1]^{2/(2-n)} - 1\big)\big]^{-1/2}\Big), \tag{5.5}$$

where h is the vertical extent of the source and β is the parameter that can be used to fit the model to the data, along with the unspecified parameter n.

For the input parameters of the analytic solution given by equation (5.5), we choose $H = 2$ m (inferred from the CTD profiles), $C_0 = 540$ p.p.b. (as noted earlier), $h = 0.91$ m, $b = 0.61$ m, and $U = 0.17\ \mathrm{m\,s^{-1}}$, the mean observed alongshore velocity in the lowest two ADCP bins during Mission 2.

Using these parameter choices, we perform a nonlinear least-squares fit using the peak concentration data from each of the transects during both the inbound and outbound legs of Mission 2 to determine the values of n, the exponent relevant for scale-dependent dispersion, and β, the constant of proportionality. It should be noted that for the few incomplete transects where the entire plume width is not measured, the data are not used since there is no reliable means of inferring the actual maximum concentration for these transects. The fit based on the 'complete' transects is shown in figure 10.

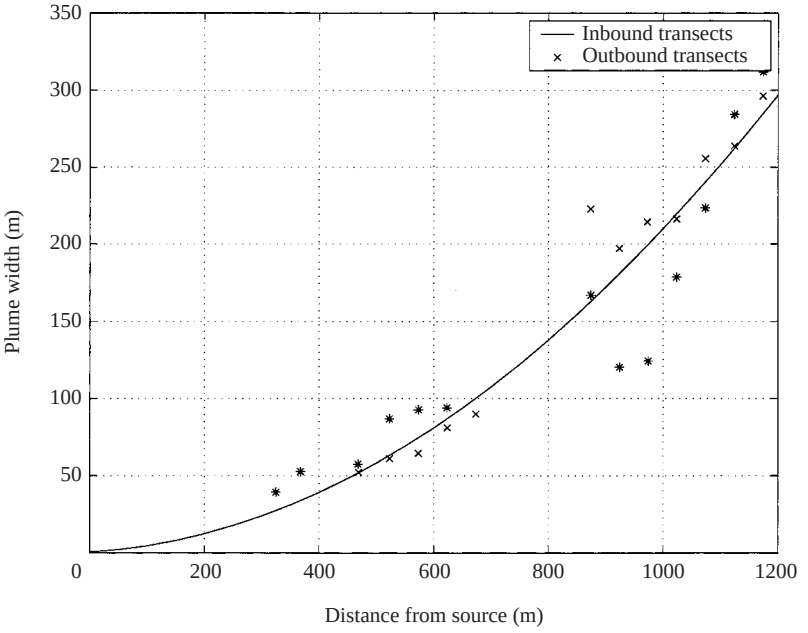

FIGURE 11. Plume width as a function of distance from source. Width data is based on the measured second moment (see equation (3.2)), and best fit is based on equation (5.7).

The best-fit solution yields $n = 1.5$ and $\beta = 0.020$ ($r^2 = 0.96$). The value for n is larger than the typically inferred 4/3 value for scale-dependent dispersion (Stommel 1949; Brooks 1960; Okubo 1971; ST2K) and suggests a strongly scale-dependent dispersive process in the lateral direction.

It is interesting to note that the peak concentration observed during the last transect of Mission 1 at a distance 150 m from the source (transect 39, about fifty minutes prior to Mission 2) is consistent with this fit (shown as a data point in figure 10, but not included in the fit).

5.2. *Longitudinal variations in plume width*

As an alternative method for estimating the plume dispersion, we make use of the longitudinal variation in plume width scale (as defined by equation (3.2) measured during Mission 2). The growth of the width of a plume is governed by equation (1.4), which, when combined with the scale-dependent dispersion coefficient (equation (5.2)) and defining $L = \sqrt{12}\tilde{y}$ (see Brooks 1960) gives

$$\frac{1}{12}\frac{\mathrm{d}L^2}{\mathrm{d}t} = 2\alpha L^n, \tag{5.6}$$

where α is a dimensional coefficient given by $\alpha = \beta U/12b^{n-1}$.

The solution to this equation (for $n \neq 2$) is found by using separation of variables and an initial condition for the plume width $L = b$ at the source location (x=0):

$$L(x) = [(2-n)\beta b^{1-n}x + b^{2-n}]^{1/(2-n)}. \tag{5.7}$$

Using a nonlinear least-squares regression for this equation with the input parameters $b = 0.61$ m and $U = 0.17\,\mathrm{m\,s^{-1}}$ and optimizing for β and n gives the best-fit shown in figure 11 ($r^2 = 0.91$) where $n = 1.5$ and $\beta = 0.024$. These values are very similar

to those obtained using the analytic solution and the observed peak concentration values, providing an independent corroboration of those results.

It is worth noting that there are other studies of scale-dependent dispersion that find n to be significantly less than 4/3 (Murthy 1976; Lawrence 1995). Lawrence, for example, finds an exponent of 1.1 when studying dispersion of an instantaneous dye release in Twin West Lake using video images of the surface layer. He attributes the lower observed exponent to the intermittency of turbulent mixing. Alternatively, the sensitivity of the rate of growth to wind speed noted in his paper suggests that wind-driven shear in the epilimnion is important in driving the observed dispersion. This process should not be scale-dependent at all, but instead should be characterized by a constant dispersion coefficient. One suspects that both the wind-driven shear dispersion and lateral turbulent motions in the surface layer would be responsible for dispersing dye in the horizontal plane. Together, these processes would result in a scale-dependent exponent somewhat less than 4/3, but still retaining some scale-dependence.

In contrast, our study focuses on lateral dispersion from a steady source, thereby isolating the dispersive process which one expects to be scale-dependent. In the next subsection, we attempt to reconcile our calculated exponent with those predicated by turbulence theories.

5.3. *Compound dispersion analysis*

The fits in the previous two subsections were based on an optimization of the exponent which defined the scale-dependence of the dispersion coefficient. The resulting exponent, $n = 1.5$ is somewhat above the value expected in typical three-dimensional turbulence ($n = 4/3$, see § 1.2.2) and below the value which would occur in two-dimensional turbulence ($n = 2$). Further, referring to equation (1.9) in the introduction, we see that a dispersion coefficient of $n = 1.5$ would occur if the energy density spectrum had a k^{-2} form ($m = 2$), which is not to be expected in the environment. However, it is important to note that the equations being optimized (equations (5.5) and (5.7) for figures 10 and 11, respectively) are singular at $n = 2$, which corresponds to the case of two-dimensional turbulence. It is likely, therefore, that the optimization algorithm would not find a global optimum, since it cannot adequately search parameter space around $n = 2$.

In fact, the far-field ($x > 800$ m) data shown in figure 11 appear to have a steeper slope than that predicted by $n = 1.5$. Further, the near-field data ($x < 800$ m) have smaller slope than the curve defined by the best-fit exponent, suggesting that there may be a transition in dynamics at $x \sim 800$ m. The distinction between these two regions suggests that a superior fit to the data may be achieved by defining a 'compound fit', with different dispersion laws in the near field and the far field. In the near field, we will fit the data using the 4/3-law, which is the scale-dependence expected in three-dimensional turbulence. In the far field, we will explore the use of a two-dimensional turbulent velocity structure, and use a plume-scale-squared ($n = 2$) law for dispersion.

In order to define this compound structure for the plume model, we first need to define the solutions for centreline concentration and plume width for the case $n = 2$, which is singular and the equations must be integrated directly, resulting in exponentials of the downstream distance. The equivalents to (5.5) and (5.7) for $n = 2$ are

$$C_{CL}(x) = C_0 \frac{h}{H} \operatorname{erf}\left(\left[\tfrac{2}{3}\left(e^{2\beta x/b} - 1\right)\right]^{-1/2}\right) \tag{5.8}$$

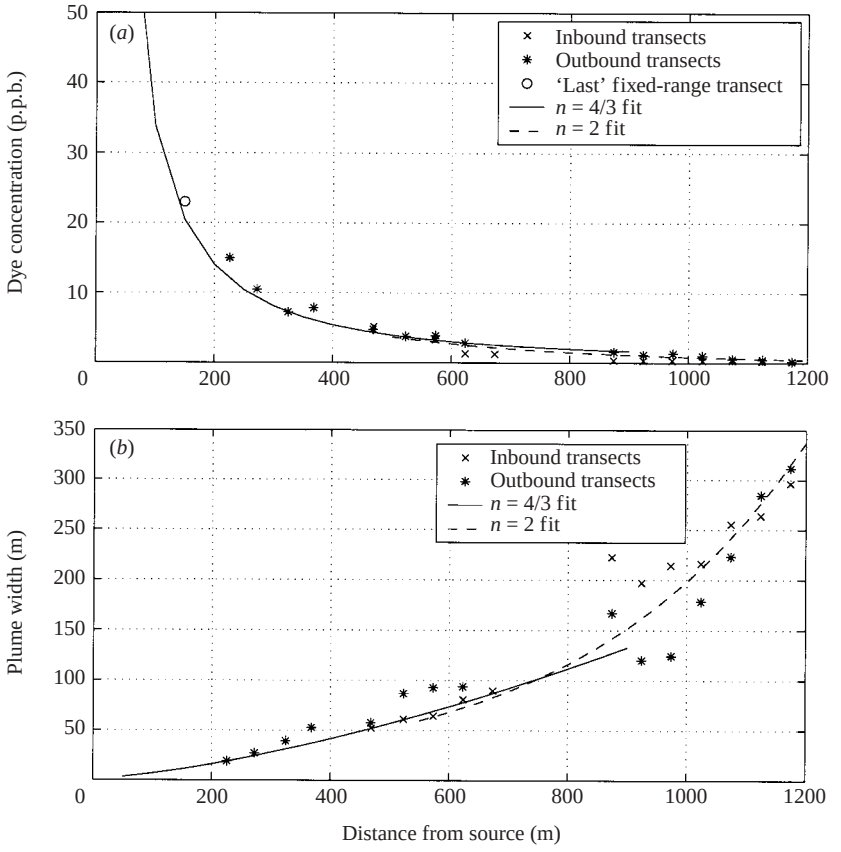

FIGURE 12. (*a*) Compound fit of centreline concentration and (*b*) compound fit of plume width, as a function of distance from source.

and

$$L(x) = b\mathrm{e}^{\beta x/b}. \tag{5.9}$$

These solutions assume that the scale-squared dispersion law applies from $x = 0$. Instead, the initial growth will be governed by the three-dimensional turbulence in the near field. In view of this, we need to define a virtual origin for the scale-squared dispersion solution, such that equations (5.8) and (5.9) become

$$C_{CL}(x) = C_0 \frac{h}{H}\ \mathrm{erf}\left(\left[\tfrac{2}{3}\left(\mathrm{e}^{2\beta(x-x_*)/b} - 1\right)\right]^{-1/2}\right) \tag{5.10}$$

and

$$L(x) = b\mathrm{e}^{\beta(x-x_*)/b}, \tag{5.11}$$

where x_* is a virtual origin which accounts for the dispersion of the plume in the initial 4/3-law region.

The optimization of this compound fit now defines three parameters: $\beta_{4/3}$, β_2 (where the subscripts denote the exponent for the scale-dependence of the dispersion coefficient) and x_*, the virtual origin for the scale-squared solution. The result of this exercise is shown in figures 12(*a*) and 12(*b*) for equations (5.10) and (5.11) respectively. In the fit to the centreline concentrations (figure 12), the values of the parameters were $\beta_{4/3} = 0.0356$, $\beta_2 = 0.0018$, and $x_* = -1040$. The fit to the lengthscale

calculations results in similar parameters: $\beta_{4/3} = 0.0356$, $\beta_2 = 0.0016$ and $x_* = -1175$. While the difference between these parameters is small, in the scale-squared region of the fit, the function is extremely sensitive to the choice of β_2, due to the exponential form.

6. Discussion

The methods of estimating the scale-dependent dispersion in §§ 5.1 and 5.2 both yield a similar value of $n = 3/2$, which is larger than previously documented by ST2K, Okubo (1971) and Brooks (1960). This value, however, may not represent the actual structure of the velocity field, but instead may represent an average over the 1200 m of plume development measured. As presented in § 5.3, a compound fit, which uses the expected values of $n = 4/3$ in the near field and $n = 2$ in the far field also fits the data well, subjectively better capturing the far-field lateral dispersion and drop in centreline concentration. It should be noted that in ST2K a bottom boundary layer which grew along the direction of the plume growth was assumed, which would have provided additional dilution of the plume and might have masked the compound structure presented here. In the following subsections, we will discuss several features of the plume structure in more depth.

6.1. *Compound scale-dependent dispersion*

In the coastal ocean, the upper layer of the ocean or in the lower atmosphere, where the vertical dimension of the flow is constrained by boundaries and density stratification, large-scale velocity fluctuations would be expected to obey the k^{-3} spectrum of Batchelor and Kraichnan. As we consider smaller and smaller scales, at some point the spectrum transitions to the $k^{-5/3}$ spectrum of Kolmogorov. Under this forcing, plume growth would be expected to follow a compound dispersion law, as presented in § 5.3.

As a plume grows downstream from its source, the growth of the scalar distribution can be thought of as the reverse of the velocity cascade (which transitions from a k^{-3} spectrum to the $k^{-5/3}$ spectrum). Initially, the plume is dispersed by three-dimensional turbulence structures, which would obey the Kolmogorov inertial-range assumption, defining a dispersion coefficient with a 4/3 power law. At some point, the plume reaches a lateral scale which is larger than the largest three-dimensional turbulent motions, and will have a lengthscale comparable to some of the two-dimensional eddy motions. At this point, the velocity fluctuations should begin to follow the Batchelor–Kraichnan inertial-range assumption, which would define a dispersion coefficient with a 2 power (scale-squared) law. If the plume were to begin to disperse under a 4/3 power law, and then transition to a 2 power law, the initial growth would be slower than the 3/2 'optimal' fit in the near field, but more rapid in the far field, consistent with the data in figures 10 and 11.

The fits in figures 12(*a*) and 12(*b*) demonstrate the effectiveness of using the compound dispersion model. While the quality of the fit for the compound fit is not that different from the individual fits in figures 10 and 11 (all $r^2 > 0.91$), the trends in the data are better represented by the compound fit. In particular, the far-field portion of the lengthscale fitting in figure 11 (using the single-exponent fit) underpredicts the dispersion of the plume for the last several data points. The compound fit in figure 12(*b*) is a superior representation of the far-field data, and extrapolation beyond 1200 m would appear to be better approached using the compound fit than the single

scale-dependence approach. Further, the compound fit represents the expectations for the structure of the velocity field, which should obey the Batchelor–Kraichnan spectrum at the large scales and the Kolmogorov spectrum at smaller scales.

The transition between the 4/3-law and the scale-squared law would be expected to occur when the plume scale exceeds the largest three-dimensional eddies by a multiplicative factor of order 1 (usually assumed to be $\sqrt{2}$ or 2). Based on the results summarized in figure 12, it appears that this occurs at approximately 700 m downstream of the source, where the lateral extent of the plume is defined by $L \approx 75$ m, which would be equivalent to a plume scale as defined in § 4 of $\tilde{y} \approx 20$ m. This value would suggest that the largest three-dimensional turbulence scales would extend about 10–15 m in the horizontal direction. This is somewhat larger than would be expected in a stratified water column, since the vertical extent would appear to be constrained to a bottom mixed layer with a height of only a few metres. This estimate for the large-eddy scale is similar, however, to the local depth, which may be providing a second – and more severe – limitation on the development of the turbulence. In general, we would expect that plume growth would transition from the three-dimensional model (4/3-law) to the two-dimensional model (scale-squared law) at a point where the plume scale exceeds the three-dimensional turbulent scales, which would be estimated by constraints defined by the local geometry and the presence of boundaries and stratification.

6.2. *Meandering versus relative dispersion*

The analysis of §§ 4 and 5 can be compared to determine the relative contribution of meandering to the overall dispersion of the plume. In § 4, a meandering dispersion coefficient, K_m, was defined for the fixed-range data to be $0.0714\ \mathrm{m^2\ s^{-1}}$. This dispersion coefficient would be additive with a constant relative dispersion coefficient, if both can be modelled with a Fickian dispersion coefficient and if a separation in scales exists between those motions creating the meanders and those setting the relative dispersion. In § 5, however, the relative dispersion is demonstrated to be scale-dependent and non-Fickian. As a result, if a Fickian dispersion coefficient is to be used, the appropriate value will depend upon the distance from the source being analysed. To be clear, the apparent Fickian dispersion coefficient for relative dispersion, K_t^f, is defined to be that dispersion coefficient that would correctly predict the plume width at a given distance downstream of the source. If the variance grew linearly, then this quantity would be a constant and the dispersion would not be scale-dependent. However, because the variance grows faster than linear, the apparent Fickian dispersion coefficient must increase as we consider distances further from the source. This variation is plotted in figure 13, which shows a rapid increase in the dispersion coefficient with distance, ranging from about $0.01\ \mathrm{m^2\ s^{-1}}$ in the near field to nearly $1\ \mathrm{m^2\ s^{-1}}$ a kilometre downstream. At a distance of approximately 600–700 m, the contribution to dispersion from relative dispersion is comparable to that from meandering, as was estimated at a distance of 150 m.

As described in § 5.3, we expect that the plume at some point transitions from being dispersed by three-dimensional motions to the large-scale two-dimensional flow structures expected in a constrained flow. At that point, the motions defining relative dispersion, which are of the same scale as the plume, are no longer uncorrelated with the large-scale motions defining the meandering. As a result, the linear decomposition of the dispersion coefficient into relative and meander components (§ 4.2) is no longer valid. The discussion of § 5.3 indicates that this transition occurs at a lengthscale of

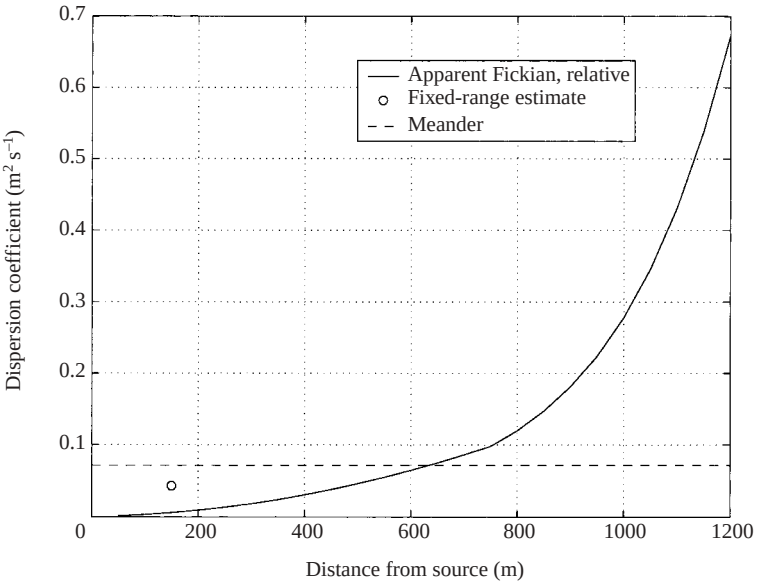

FIGURE 13. Dispersion coefficient decomposed into meandering and Fickian centreline constituents as a function of distance from source.

approximately 800 m from the source. Examination of figure 13 suggests that this coincides with the point at which the apparent Fickian dispersion starts to exceed the meander dispersion significantly (approximately a factor of 2 by 800 m). In the near field, therefore, a fluctuating plume model that accounts for both relative and meander dispersion components is appropriate; in the intermediate and far field, the meander-induced dispersion becomes less significant and a non-fluctuating plume model with a scale-squared dispersion law appears to be the appropriate choice.

The point at which the dispersion transitions from a fluctuating plume model (with a 4/3-law to describe the growth around the centreline) to one dominated by scale-squared dispersion will depend on the magnitude and timescales of the motions defining the meandering, which will be related to the scales that define the transition from three-dimensional turbulence to two-dimensional flow structures. As was demonstrated in § 4.3, a simple model of dispersion using streaklines defined from a velocity time series at a location near the source is successful at predicting the meandering dispersion coefficient. Because the meandering is being driven by large-scale motions, this (Fickian) coefficient should be constant over the plume development. As a result, the equation defining the rate of growth of the lateral variance of the plume due strictly to meandering can be integrated to give

$$\tilde{y}_m^2 = 2K_m x/U + \tfrac{1}{12}b^2, \tag{6.1}$$

where $\tilde{y}_m$ is the lateral scale of the meandering process. Equivalence between the two contributions to dispersion is at the point where this meandering scale ($\tilde{y}_m$) is comparable to the instantaneous plume width ($\tilde{y} = L/\sqrt{12}$), which is predicted using the scale-dependent formulation presented in § 5.3. For this experiment, this occurs approximately 600–700 m from the source, where the plume has a lateral extent of approximately 20 m.

7. Summary and conclusions

In the coastal ocean or the lower atmosphere, the vertical component of velocity fluctuations is constrained by the presence of stratification and solid boundaries. Not only does this restrict the vertical dispersion of scalars, but it also forces large-scale velocity fluctuations to be essentially two-dimensional (in the horizontal plane), altering the form of plume dispersion at those scales.

The plume analysed here is characterized by both a variable centreline position (i.e. a meandering plume) and a scale-dependent growth of the plume around the centreline. A simple model of the meandering process, which assumes that the velocity fluctuations creating the meander are of very large scale (and constant over the scale of plume development) is quite successful at predicting the lateral variation in the position of the plume centreline. The equivalent (Fickian) dispersion coefficient is estimated as 0.0714 $m^2 s^{-1}$ for these data, but could be reliably estimated from the temporal variability in lateral flow velocities at other sites. The success of this uniform velocity model implies that the velocity fluctuations defining the plume meander are of very large scale – much larger than the lateral plume scale – and the meander dynamic can be linearly separated from the growth of the plume around the centreline.

The growth of the plume around this variable centreline is defined by a scale-dependent dispersion coefficient, where the rate of growth of the plume depends on the plume scale itself. This is to be expected whenever a scalar cloud is being dispersed by a velocity field characterized by a range of lengthscales that include the scale of the scalar distribution itself. In a three-dimensional turbulent field, the scale-dependence should be characterized by an exponent of 4/3. In a two-dimensional flow, the exponent would become 2 (or the dispersion would obey a scale-squared law). In the observations presented here, using a single exponent to describe the dispersion process resulted in a value for the exponent that was intermediate between these two values. This result is due to the fact that the transition from three-dimensional turbulent dispersion to two-dimensional lateral dispersion occurs within the region of the observations. As a result, the initial dispersion is governed by a 4/3 power law, while the far field dispersion is governed by a scale-squared dispersion law. The use of a compound model of dispersion that explicitly accounts for this transition appears to be superior to a single model of dispersion using an intermediate exponent, particularly if extrapolations into the far field are to be made.

To summarize, the dynamics of this highly variable plume can be described by and separated into two processes: a meandering plume and scale-dependent growth of the plume around the centreline. The largest two-dimensional scales cause the plume to meander. These motions can be well-represented by a single measurement in the vicinity of the plume (§4.3). Around that centreline, the plume growth is governed by a scale-dependent dispersion coefficient which transitions from a 4/3-exponent, the value expected for three-dimensional turbulence, to a scale-squared behaviour, which is expected in the presence of two-dimensional velocity fluctuations.

In the analysis of scalar transport in the environment, either long-term averages or peak concentrations or both may be significant. For example, in the consideration of larval dispersion, the average concentration over a period of time relevant for settling may be most important. On the other hand, for the problem of contaminant dispersal and ecosystem response to toxic discharges, the instantaneous peak concentrations are a dominant consideration. By resolving both the meandering of the plume and the growth of the plume around its centreline, as in the analysis presented here, both of these considerations can be addressed and the complexity of the plume structure can be approximated.

The datasets presented here would not have been possible without the extraordinary assistance of R. Arrieta and SPAWAR Systems Center of San Diego, J. Deschamps (NRL), P. Holland (Thorleaf Research), Arete Associates, and the technical staff at the Field Research Facility. The authors also wish to thank K. Ward of ONR for his generous support of the CSME science program (N00014-98-1-0785 and N00014-01-1-1012). MTS acknowledges the support of ONR (N00014-01-1-0469) and NSF (OCE-0094317) during the final preparation of this manuscript. Finally, the authors thank the three anonymous reviewers who helped improve both the content and clarity of the paper.

REFERENCES

Austin, J. A. & Lentz, S. J. 2002 The inner shelf response to wind-driven upwelling and downwelling. *J. Phys. Oceanogr.* **32**, 2171–2193.

Bara, B. M., Wilson, D. J. & Zelt, B. W. 1992 Concentration fluctuation profiles from a water channel simulation of a ground-level release. *Atmos. Environ.* **26A**, 1053–1062.

Batchelor, G. K. 1952 Diffusion in a field of homogeneous turbulence II. The relative motion of particles. *Proc. Camb. Phil. Soc.* **48**, 345–362.

Batchelor, G. K. 1969 Computation of the energy spectrum in homogeneous two-dimensional turbulence. *Phys. Fluids Supp.* II, 233–239.

Brooks, N. H. 1960 Diffusion of sewage effluent in an ocean-current. *Proc. First Intl Conf. on Waste Disposal in the Marine Environment, UC, Berkeley.*

Csanady, G. T. 1973 *Turbulent Diffusion in the Environment*. D. Reidel.

Fackrell, J. E. & Robins, A. G. 1982 Concentration fluctuations and fluxes in plumes from point sources in a turbulent boundary layer. *J. Fluid Mech.* **117**, 1–26.

Fischer, H. B., List, E. J., Koh, R. C. Y., Imberger, J. & Brooks, N. H. 1979 *Mixing in Inland and Coastal Waters.* Academic.

Gifford, F. A. 1959 Statistical properties of a fluctuating plume dispersion model. *Adv. Geophys.* **6**, 117–137.

Gifford, F. A. 1960 Peak to average concentration ratios according to a fluctuating plume dispersion model. *Intl J. Air Pollut.* **3**, 253–260.

Hill, A. E. 1991 Advection-diffusion-mortality solutions for investigating pelagic larval dispersal. *Mar. Ecol. Prog.* **70**, 117–128.

Kraichnan, R. H. 1967 Intertial ranges in two-dimensional turbulence. *Phys. Fluids* **10**, 1417–1423.

Kraichnan, R. H. 1971 Inertial-range transfer in two- and three-dimensional turbulence. *J. Fluid Mech.* **47**, 525–535.

Kristensen, L., Jensen, N. O. & Petersen, E. L. 1981 Lateral dispersion of pollutants in a very stable atmospher – the effect of meandering. *Atmos. Environ.* **15**, 837–844.

Large, W. G. & Pond, S. J. 1981 Open ocean momentum flux measurements in moderate to strong winds. *J. Phys. Oceanogr.* **11**, 324–336.

Lawrence, G. A. 1995 Natural dispersion in a small lake. *Limnol. Oceanogr.* **40**, 1519–1526.

Lentz, S. J. 1995 Sensitivity of the inner-shelf circulation to the form of the eddy-viscosity profile. *J. Phys. Oceanogr.* **25**, 19–28.

Lentz, S. J. 2001 The influence of stratification on the wind-driven cross-shelf circulation over the North Carolina shelf. *J. Phys. Oceanogr.* **31**, 2749–2760.

Murthy, C. R. 1976 Horizontal diffusion characteristics in Lake Ontario. *J. Phys. Oceanogr.* **6**, 76–84.

Okubo, A. 1971 Oceanic diffusion diagams. *Deep-Sea Res.* **18**, 789–802.

Richardson, L. F. 1926 Atmospheric diffusion shown on a distance-neighbour graph. *Proc. R. Soc. Lond.* A **110**, 709–737.

Roberts, P. J. W. 1999 Modeling Mamala Bay outfall plumes. II: Far-field. *J. Hydraul. Engng* **125**, 574–583.

Sawford, B. L. & Stapountzis, H. 1986 Concentration fluctuations according to fluctuating plume models in one and two dimensions. *Boundary-Layer Met.* **37**, 89–105.

Stacey, M. T., Cowen, E. A., Powell, T. M., Dobbins, E., Monismith, S. G. & Koseff, J. R. 2000 Plume dispersion in a stratified, near-coastal flow: measurements and modeling. *Contine. Shelf Res.* **20**, 637–663 (referred to herein as ST2K).

Stokes, G. G. 1847 On the theory of oscillatory waves. *Trans. Camb. Phil. Soc.* **8**, 441–445.

Stommel, H. 1949 Horizontal diffusion due to oceanic turbulence. *J. Mar. Res.* **8**, 199–225.

Taylor, G. I. 1953 Dispersion of solute matter in solvent flowing slowly through a tube. *Proc. R. Soc. Lond.* A **219**, 186–203.

Tennekes, H. & Lumley, J. L. 1972 *A First Course in Turbulence*. The MIT Press.

Turner, D. B. 1970 *Workbook of Atmospheric Dispersion Estimates*. Environmental Protection Agency, North Carolina.

Turner, J. S. 1973 *Buoyancy Effects in Fluids*. Cambridge University Press.

Vasholz, D. P. & Crawford, L. J. 1985 Dye dispersion in the seasonal thermocline. *J. Phys. Oceanogr.* **15**, 695–712.